Chen *et al. Cancer Cell International* (2026) 26:213
https://doi.org/10.1186/s12935-026-04299-y

Cancer Cell International

RESEARCH Open Access

Single-cell transcriptomics uncovers heterogenous cell clusters and the biomarker FUT11 in ovarian cancer progression

Qi Chen[1], Zhibin Liu[1], Junpei Wang[1], Yu Teng[1], Mei Jiang[1*] and Wentao Yue[1*]

Abstract

Background: Ovarian cancer (OC) is the most lethal of gynecological cancers and presents a poor prognosis due to difficulty in early diagnosis, extensive abdominal metastasis and chemo-resistance. We utilized single-cell transcriptomics to deconvolute intratumoral heterogeneity and identify biomarkers and therapeutic targets.

Methods: Single-cell RNA sequencing (scRNA-seq) were performed with 15 patient samples. Metastatic and chemo-resistant epithelial subclusters were discovered by copy-number variations (CNV), Kaplan–Meier and enrichment analysis. Fucosyltransferase 11 (FUT11) was identified by differential expression analysis and validated by in vitro assays. Cell-cell communication analysis and protein–protein interaction (PPI) network were conducted to discover pathways and receptors in FUT11 positive (FUT11+) cells. Function of FUT11 in transforming growth factor-β (TGF-β) pathway and drug response prediction were analyzed.

Results: Epithelial subcluster EC5 was associated with metastasis, chemo-resistance and poor prognosis of OC. FUT11 was a hub gene of EC5 and communicated with mesenchymal cells through TGF-β receptors to regulate downstream genes. FUT11 could be applied in chemo-resistance prediction and drug discovery.

Conclusions: The present research provided new insights into gene signatures for tumor progression and drug discovery, and identified FUT11 as a diagnostic biomarker and therapeutic target.

Keywords Ovarian cancer, Single-cell transcriptomics, FUT11, Epithelial subcluster, Tumor microenvironment, TGFBR1, Precision medicine

Introduction

OC is the most lethal of all gynecological cancers, and high-grade serous ovarian cancer was the most lethal OC subtype [1]. The high mortality rate and poor prognosis of OC can be explained by tendency for late diagnosis, extensive abdominal metastasis, an immunosuppressive tumor microenvironment (TME), significant adverse reactions and resistance to chemotherapy [2–4]. However, the pathogenesis of OC remains unclear. In order to improve the treatment effect of OC, it is an urgent need to clarify the relevant mechanism, find effective diagnostic markers and therapeutic targets for OC.

*Correspondence:
Mei Jiang
jiangmei627@ccmu.edu.cn
Wentao Yue
yuewt@ccmu.edu.cn
[1]Central Laboratory, Beijing Obstetrics and Gynecology Hospital, Capital Medical University. Beijing Maternal and Child Health Care Hospital, No.17, Qihelou Street, Dongcheng District, Beijing 100006, PR China

Table 1 Sample information

ID	Pathology	Tissue source	Age	FIGO stage	Drug response	Accession number	Sample number
NM1	Normal	Ovary	60–65	N/A	N/A	E-MTAB-8107	scrSOL007
PT1	HGSOC	Ovary	N/A	N/A	N/A	GSE130000	P1
PT2	HGSOC	Ovary	70–75	IIIc	N/A	E-MTAB-8107	BT1307
PT3	HGSOC	Ovary	N/A	N/A	N/A	GSE158937	GSM4816045
PT4	HGSOC	Ovary	N/A	N/A	N/A	GSE158937	GSM4816046
PT5	HGSOC	Ovary	N/A	N/A	N/A	GSE158937	GSM4816047
PT6	HGSOC	Ovary	58	IIIc	Resistant	GSE201047	1_N_OT_PT1
PT7	HGSOC	Ovary	48	IIIb	Responsive	GSE201047	16_N_OT_PT3
MT1	HGSOC	Peritoneum	N/A	N/A	N/A	GSE130000	M1
MT2	HGSOC	Peritoneum	70–75	IIIc	N/A	E-MTAB-8107	BT1305
MT3	HGSOC	Peritoneum	50–55	IVb	N/A	E-MTAB-8107	scrSOL001
MT4	HGSOC	Peritoneum	60–65	IVb	N/A	E-MTAB-8107	scrSOL003
MT5	HGSOC	Peritoneum	80–85	IVb	N/A	E-MTAB-8107	scrSOL004
MT6	HGSOC	Peritoneum	58	IIIc	Resistant	GSE201047	3_N_PER_PT1
MT7	HGSOC	Peritoneum	48	IIIb	Responsive	GSE201047	18_N_PER_PT3

HGSOC: high-grade serous ovarian cancer

Recently, scRNA-seq technology has been used to provide insights into cellular compositions and heterogeneity of tumor microenvironment across various types of cancer [5, 6]. A subgroup of malignant epithelial cells (EpiCs) with elevated TOP2A expression showed heightened sensitivity to neoadjuvant chemotherapy [7]. Dendritic cell-derived CXCL10 was reported to play a pivotal role in restraining OC growth and metastasis through cytotoxic T lymphocytes activation [8]. S100A9+ tumor cell subtype and metabolic alterations was identified in CAFs and TAMs, shedding light on mechanisms of high-grade serous ovarian cancer progression [9]. However, more detailed molecular characterization and biomarkers for OC still need to be uncovered.

In this study, we constructed a cell atlas of OC through integrating scRNA-seq data from 15 patient samples, and discovered a metastatic and chemo-resistant epithelial subcluster EC5 associated with poor prognosis of OC. FUT11 was a hub gene of EC5. FUT11 is a member of the α–1,3-FUT subfamily, resides on the Golgi membrane and links alpha-l-fucose onto conalbumin glycopeptides and biantennary N-glycan acceptors [10]. Although a range of FUTs in other subfamilies have gained attention as promising targets closely related to cancer progression and prognosis [11–13], very few studies have been conducted around FUT11 in OC, especially for its application in precision medicine. FUT11 was identified as a biomarker in a few kinds of tumors such as colon adenocarcinoma [14], stomach adenocarcinoma [15], breast cancer (BC) [16], and cervical squamous cell carcinoma [17]. In pancreatic cancer, hypoxia-induced FUT11 promoted proliferation and metastasis through maintaining the stability of PDK1 and activation of AKT/mTOR signaling pathway [18]. In hepatocellular carcinoma cells, FUT11 functioned as a target gene of HIF1α in proliferation and mobility [19]. FUT11 also promoted gastric cancer (GC) proliferation by targeting GPX4 to inhibit ferroptosis [20] or through the PI3K/AKT signaling pathway [21]. We previously found that FUT11 was related with EMT process [22]. In the present study, we verified the effects of FUT11 on promoting OC progression, and association of FUT11 with worse prognosis. We elucidated how FUT11 communicated with TME cells and its potential application in chemo-resistant prediction and drug discovery.

Table 2 Clinic information of tumor samples

	Total (N=14)	Primary (N=7)	Metastasis (N=7)	P
Age				0.388
<55	3 (21.4%)	1 (14.3%)	2 (28.6%)	
>55	6 (42.9%)	2 (28.6%)	4 (57.1%)	
N/A	5 (35.7%)	4 (57.1%)	1 (14.3%)	
Stage				0.170
III	6 (42.9%)	3 (42.9%)	3 (42.9%)	
IV	3 (21.4%)	0 (0.0%)	3 (42.9%)	
N/A	5 (35.7%)	4 (57.1%)	1 (14.3%)	
Drug response				1.000
Responsive	2 (14.3%)	1 (14.3%)	1 (14.3%)	
Resistant	2 (14.3%)	1 (14.3%)	1 (14.3%)	
N/A	10 (71.4%)	5 (71.4%)	5 (71.4%)	

Materials and methods

scRNA-seq data processing

The scRNA-seq datasets were obtained from the Gene Expression Omnibus (GEO) [23, 24] with accession numbers GSE130000, GSE201047, GSE158937, and the BioStudies database [25, 26] under accession number E-MTAB-8107 (Tables 1 and 2).

Further quality control was applied to filter cells using the following criteria: 400 < detected genes < 5000,

mitochondrial gene percent < 15%, hemoglobin gene percent < 0.1% and ribosomal gene percent > 1%. Then we removed genes expressed in less than 3 cells. Subsequently, cells were integrated by Harmony method using the 'IntegrateLayers()' function of R package 'Seurat' [27].

Markers for annotation of cell types included: EPCAM, KRT19 and CLDN4 for EpiCs; COL1A1, COL1A2 and DCN for fibroblasts; PECAM1, VWF and CDH5 for endothelial cells; CD79A and IGHG3 for B cells; CD3D, CD3E and CD2 for T cells; as well as FCER1G, CD14 and CD68 for myeloid.

The EpiCs were subdivided into 16 subclusters. Heatmap representation was generated using 'ComplexHeatmap' package. Relative expression of samples for each gene was depicted in color-code, with intensities varied from red (for upregulated genes) to blue (for downregulated genes).

The CNVs estimation

The CNVs were estimated by the 'infercnv' package (v1.20.0; Tickle et al., 2019). The B cells, T cells, myeloid cells, endothelial cells and normal EpiCs were used as reference. The CNV scores were obtained by accumulating the CNV levels of cells within each subcluster.

Bulk RNA-seq analysis

The bulk RNA-seq data and phenotype metadata were downloaded from UCSC XENA Treehouse [28, 29], consisting of 88 normal ovary samples from the Genotype-Tissue Expression (GTEx) project and 374 OC samples from the Cancer Genome Atlas (TCGA). Data was integrated by R software packages.

Survival analysis

Expression profiles of the top 30 marker genes for each subcluster were extracted and the feature scores of 374 OC patients from the TCGA cohort were calculated by gene set variation analysis (GSVA). Combining with the overall survival (OS) time, the Kaplan–Meier and log-rank tests were applied to construct and compare survival curves using the 'survival' package (v3.7-0; Therneau, 2020). Cox regression analysis was performed to identify prognostic-related subclusters or genes.

Gene set functional analysis

The gene set functional enrichment was conducted with package 'clusterProfiler' [30] and 'GSVA' [31]. Kyoto Encyclopedia of Genes and Genomes (KEGG) and MSigDB database were used for gene set enrichment analysis (GSEA). The Gene ontology (GO) enrichment analysis was applied for trajectory analysis.

Single-cell trajectory analysis

Trajectories within the epithelial subclusters were constructed using the monocle package (v2.34.0) [32]. UMI count matrices and the negbinomial.size parameter were used to create a CellDataSet object in the default setting. The top 30 markers of each subcluster were used for semisupervised trajectory construction. The DDRTree method and the 'orderCells' function were used for dimensional reduction and cell ordering. The branch with normal EpiCs at the start point and containing more cells from primary samples was chosen as the start of pseudotime for further analysis. Genes were clustered along trajectory. Genes with branch-dependent expression dynamics were calculated using the BEAM test in Monocle2. Genes with a q < $1x10^{-4}$ were plotted in heatmaps.

Cell–cell communication analysis

Cell–cell communications were visualized using 'CellChat' package [33]. For analysis, 5000 cells from each cell cluster were selected randomly by function 'subset'. Cellchat databases including 'Secreted Signaling', 'ECM-Receptor' and 'Cell–Cell Contact' were used.

Functional and network analysis

Data of 374 tumor samples was used for selection of DEGs correlated with FUT11, predicted with the Spearman's correlation coefficient > 0.4 and p-value < 0.05.

The PPI network were constructed using Cytoscape 3.9.1 [34]. Hub genes within the PPI network were identified using the CytoHubba plugin.

Cell culture

OC cell lines SK-OV-3 was purchased from the China Infrastructure of Cell Line Resource, and HEY was from the Beijing Chest Hospital, Capital Medical University, China. Normal ovarian cell line OSE was provided by the Obstetrics & Gynecology Hospital of Fudan University, China. These cells were maintained in RPMI-1640 culture media (Hyclone, USA) supplemented with 10% Fetal bovine serum (FBS, Life Technologies, USA) and Penicillin-Streptomycin Liquid (100X, Solarbio, Beijing, China), and incubated in a 5% CO2 humidified atmosphere at 37°C.

RNA extraction and quantitative real-time PCR (qPCR)

Total RNA was extracted from cells by RNA-Quick Purification Kit (Yishan Biotechnology Co., Ltd, China). One microgram of total RNA was reverse transcribed to cDNA by Transcript One-Step gDNA Removal and cDNA Synthesis SuperMix (Transgene biotech, Beijing, China). The qPCR was carried out using the TransStart Top Green qPCR SuperMix (+Dye II) (Transgene biotech, Beijing, China) with the Applied Biosystems 7500

Real Time PCR System (Applied Biosystems, CA, USA). GAPDH was used as a reference gene for normalization. Gene expression was calculated by the 2-△△ CT method and presented as Mean±Standard deviation. Primers used for qPCR were as follows: GAPDH-F: 5'-GAGTC AACGGATTTGGTCGT-3'; GAPDH-R: 5'-TTGATTT TGGAGGGATCTCG-3'; FUT11-F: 5'-CCTCAGAAG CTGGCAGAGTT-3'; FUT11-R: 5'-CGAGCCAGTTC GTAGTCACA-3'; TGFBR1-F: 5'-ACGGCGTTACAGT GTTTCTG-3'; TGFBR1-R: 5'-GCACATACAAACGGC CTATCTC-3'; ZEB1-F: 5'-CAGGGAGGAGCAGTGA AAGA-3'; ZEB1-R: 5'-CTCTTCAGGTGCCTCAGGA A-3'; TWIST1-F: 5'-AGTCTTACGAGGAGCTGCAG-3'; TWIST1-R: 5'-AGGAAGTCGATGTACCTGGC-3'.

RNA interference and TGF-β induction

For RNA interference, $3x10^5$ cells were seeded in 6-well plates one day before transfection. Complexes of 3.75 μ L Lipofectamine 3000 (Invitrogen, USA) and 2.25 μg FUT11 siRNA or scramble siRNA (RiboBio, Guangzhou, China) were formed in Opti-MEM I Reduced Serum media (Invitrogen, USA), incubated at room temperature for 5 min, and delivered into cell medium according to the protocol. Sequences of FUT11 siRNAs were as follows: siRNA1: 5'-GCUUUCUUGUCCCGCUAUA-3'; siRNA2: 5'-GUAGACUCCUACGGGAAAU-3'; siRNA3: 5'-GGAAGAGAUUCCUGAGAAU-3'. Scramble siRNA was used as control and the sequence was 5'-UUCUCCG AACGUGUCAGGUTTUCCAGGTCUAGTT-3'.

Cells were transfected with FUT11 siRNA (si-FUT11 group) or control siRNA. Cells were harvested for qPCR or western-blot 48 h later. For the TGF-β 1 (TGFB1)-treated group, cells were supplemented with 10 ng/mL TGFB1 (PeproTech, USA).

Western-blot

Cells were washed twice with PBS, harvested and lysed in RIPA buffer (Biosharp, China) supplemented with protease inhibitor cocktail tablets (Roche Diagnostics, NY, USA), and incubated on ice for 10 min. Protein samples were centrifuged at 15000xg for 15 min, and then were denatured with 5xloading buffer at 100°C for 10 min. Equal amount of protein were separated by 10% sodium dodecyl sulfate-polyacrylamide gel electrophoresis. Electrophoresis was performed with Tris-glycine running buffer (Biosharp, China) under 80 V for 30 min and then changed to 120 V. Proteins were transferred onto 0.45 μ M Immobilon-P PVDF Membranes (Millipore, Billerica, MA) with transfer buffer (Leagene, China) under 220 mA for 45 min. The membranes were blocked with 5% BSA in TBS and 0.1% Tween-20 (TBST) at room temperature for 1 h, and then incubated with primary antibodies against FUT11 (Abcam, USA, dilution 1:500) and β-actin (Cell Signaling Technology, USA, dilution 1:1000) at 4°C overnight. After three washes in TBST, the membranes were incubated with HRP-labeled secondary antibody (Cell Signaling Technology, USA, dilution 1:7500) for 2 h at room temperature, and then washed three times with TBST. Immobilon western chemilum HRP substrate (Millipore, Billerica, MA) was used to induce the chemiluminescence signal, which was visualized by the Chemi-Doc™ XRS+ System with Image Lab™ Software (BioRad Laboratories).

Invasion and migration assay

For analysis of the invasion ability, cells were first treated with FUT11 siRNA or control siRNA. Cells were trypsinized 48 h after transfection, and $7x10^4$ cells were seeded in the top of the 24-well transwell chambers (Costa, Massachusetts, USA) which had been coated with 10 μ g/mL Corning Matrigel Basement Membrane Matrix (CMBBM, BD Biosciences) and rehydrated with RPMI-1640 at 37°C for 30 min. Cells in the top chamber were cultured with RPMI-1640 containing 0.2% BSA, supplemented with or without TGFB1 as mentioned. In the lower compartment, RPMI-1640 supplemented with 10% FBS was used as chemoattractant. After 48 h incubation, non-invaded cells on the upper surface of the filter were removed using a cotton swab, and cells migrated through the membrane were fixed and stained using 0.1% Crystal Violet in methanol, and then photographed by a microscope. The number of invaded cells was counted.

For migration assays, the top transwell chamber was not coated with CMBBM. 10^4 cells were allowed to migrate, stained and counted as described above.

Immunofluorescence (IF) staining

$3x10^3$ cells treated with FUT11 or control siRNA were seeded in 96-well glass-bottom plates (P96-1.5H-N, Cellvis, Mountain View, CA) and cultured in RPMI-1640 without FBS, supplemented with or without 10 ng/mL TGFB1. Cells were fixed in 4% paraformaldehyde (Biosharp, China) for 30 min at room temperature, permeabilized with 0.05% Triton X-100 (Biofroxx, Germany) for 10 min, and blocked with 5% BSA/TBST for 1 h at room temperature. The fixed and permeabilized cells were incubated with primary antibodies against phosphorylated SMAD family member 3 (p-SMAD3, Cell Signaling Technology, USA, dilution 1:100) at 4°C overnight, and washed 3 times for 5 min with TBST. Antibody binding was detected with FITC-labeled secondary antibodies (Solarbio, China, dilution 1:10). Nucleus was stained with 1.25 μg/mL DAPI (Leagene, China) for 15 min, then washed with TBST. Stained cells were imaged with 60X magnification objective by the Thermo Scientific CellInsight CX7 High Content Screening Platform (Thermo Fisher Scientific, USA). Images were acquired

under 386 nm excitation light for DAPI staining, and 485 nm for FITC.

Drug response prediction and drug selection

Data of OV cell lines from CTRP2, GDSC1 and GDSC2 datasets was used as training set for ridge regression model development. The 'oncoPredict' package was used to predict the drug response of OC patients in TCGA. Half-maximal inhibitory concentrations (IC50) of the drugs were used to present drug sensitivity data. Patients were divided into high and low groups according to median expression of FUT11. Drugs differed between the FUT11-high and FUT11-low subgroups ($p < 0.05$) were selected.

Statistical analysis

To evaluate the ability of invasion and migration, experiments were repeated three times. Data was analyzed using the GraphPad Prism 9.0 statistical software by Student's t test, presented as mean ± standard deviation. Gene expression analysis was performed using Wilcoxon rank-sum test. Statistical significance was assessed at the $p < 0.05$ level.

Results

Single-cell expression atlas of OC during tumor progression

After quality control and filtration, a total of 53311 single cells from 15 samples (including seven primary OC samples, seven peritoneum metastatic tissue and one normal ovarian epithelium) were retained for subsequent analysis (Fig. 1A). We integrated these cells using Harmony to remove the batch effect, performed graph-based clustering and marker-based annotation to define each cluster. All cells were classified into 6 major cell types including EpiCs, fibroblasts, endothelial cells, B cells, T cells and myeloid, according to the uniform manifold approximation and projection (UMAP) method (Fig. 1B, C, D). Compared with primary OC tumors, the metastatic tumors had lower composition of mesenchymal cells and higher composition of immune cells, indicating heterogeneity of the TME in different pathological states (Fig. 1E).

Characterization of EpiCs and identification of metastasis- and prognosis-related EC5

We further separated all tumor EpiCs into 16 subclusters and performed CNV analysis with reference cells of endothelial cells, immune cells (myeloid cells, T cells and B cells), and EpiCs in normal samples (Fig. 2A). The CNV scores of subcluster EC11 and EC12 were similar as that of reference cells, indicating them as normal EpiCs (Fig. 2B). EC2 had a level of CNVs between reference cells and malignant cells (Fig. 2B, right). Other subclusters had obviously higher CNV scores than that of reference cells, attracting great interests as they might have higher malignant potential (Fig. 2B).

Among the malignant subclusters, EC4, EC6 and EC8 mainly presented in primary sites, while EC1, EC5, EC7, EC10, EC13, EC14 and EC15 had increased cell proportion during progression from primary to metastatic status (Fig. 2C). As heterogeneity of malignant cells resulted in different metastatic behavior, we focused on the 7 subclusters that had higher composition in metastasis than primary samples.

Relationship of these malignant and metastatic subclusters with prognosis were analyzed using the bulk RNA-seq data and clinical data from the TCGA. We identified EC5 negatively associated with OS time, EC7, EC13 and EC14 positively associated with OS time, while other subclusters with no significant relationship with prognosis (Fig. 2D, E). Taken together, we identified a specific subcluster EC5 that was related with metastasis and worse prognosis.

EC5 communicated with mesenchymal cells in TME

Different cancer subclusters might be associated with distinct biological processes, we then performed GSEA using KEGG gene sets to gain insight into the biological processes associated with subcluster EC5. EC5 enriched in carbohydrate metabolism pathways, ligand/cytokine-receptor interaction related pathways, and some signaling pathways such as HIF, TGF-β, hormone and cAMP (Fig. 3A). Investigation of this subcluster might help in understanding mechanisms of OC progression.

Next, we performed cell-cell communication analysis for interactions between subcluster EC5 and the TME cells. In metastatic tumors, subcluster EC5 had a high cell interaction strength with mesenchymal cells (including endothelial cells and fibroblasts), but a low cell interaction strength with immune cells (Fig. 3B). When compared metastatic samples with primary samples, cell interaction between EC5 and mesenchymal cells increased while cell interaction with immune cells decreased (Fig. 3C). This was consistent with the increase of EC5 in chemo-resistant samples compared with chemo-sensitive samples (Fig. 3D). These indicated that EC5 communicated with mesenchymal cells and could escape immune response.

To identify biomarkers for OC, we analyzed the top 30 markers of subcluster EC5 and identified 13 hub genes negatively associated with prognosis using the bulk RNA-seq data and clinical data from the TCGA (Fig. 3E). These hub genes were interesting for further investigation of communication of EpiCs with TME during cancer progression.

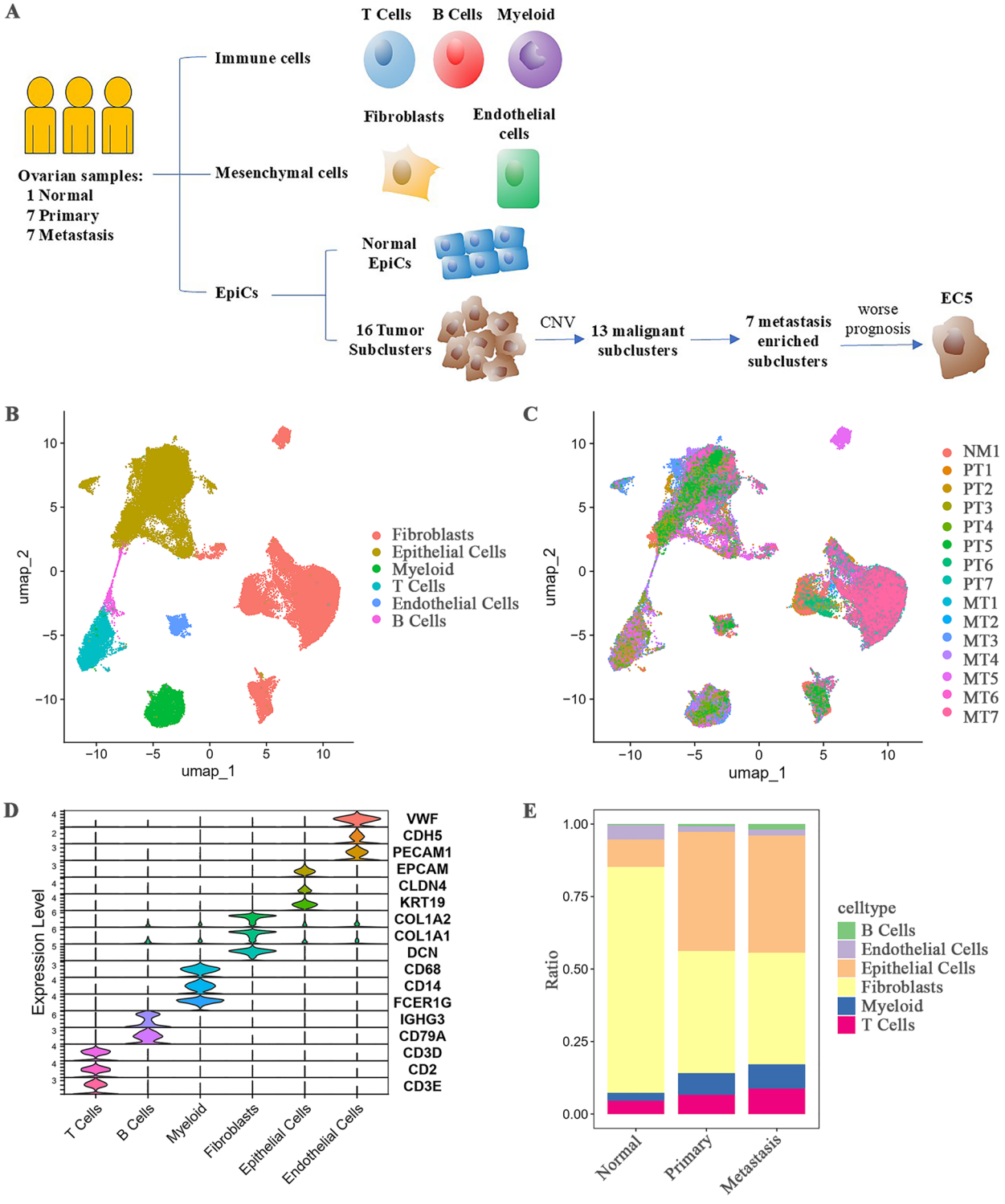

Fig. 1 Single cell expression atlas of OC. **A**. Analysis workflow of ovarian samples to identify metastasis-related epithelial subclusters. **B-C**. UMAP of single cells of OC. Colored by cell type (**B**) or patient (**C**). **D**. Violin plot of the markers of each cell type. **E**. Bar plot of the cell proportion among normal, primary and metastatic samples

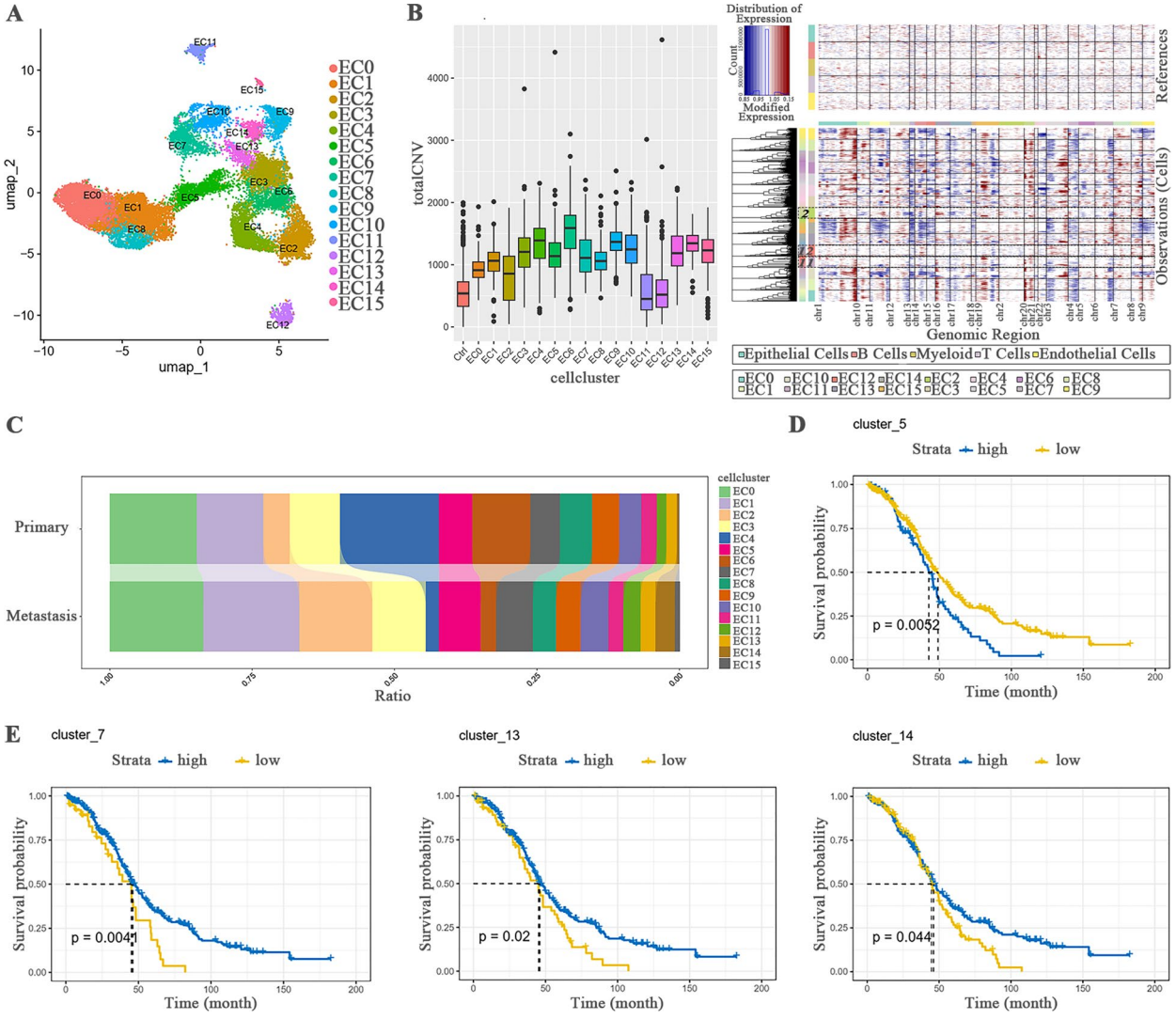

Fig. 2 Characterization of EpiCs and identification of metastasis- and prognosis-related EC5. **A**. UMAP of 16 epithelial subclusters. **B**. Differences in CNV scores (left) and chromosomal landscape of CNVs (right) among epithelial subclusters. 13 subclusters with high CNV scores were considered malignant. **C**. Cell proportion of different epithelial subclusters between primary and metastasis. 7 malignant subclusters were enriched in metastasis. **D-E**. Kaplan-Meier analysis of patients from TCGA cohort with high (blue) and low (yellow) GSVA scores based on the top 30 markers of malignant subclusters. EC5 was negatively associated with OS time (**D**), while EC7, EC13 and EC14 positively associated with OS time (**E**)

FUT11 was a prognostic biomarker elevated during OC progression

To identify genes associated with the differentiation paths across the multilineages among EpiCs, we performed a pseudotime trajectory analysis. The trajectory revealed a transcriptional hierarchy originated from normal EpiCs, transited from a state dominated by primary EpiCs toward divergent differentiation states (Fig. 4A). Genes of cells in fate 1 enriched in immune-related biological processes such as humoral immune response, and response to chemical, type I interferon or some kinds of organism (Fig. 4A, B Cluster 3). Tumor cells interacted with immune cells or secreted biomolecules to shape an immune suppressive microenvironment facilitating metastasis. Cells in fate 1 might proceed through the metastatic cascade by escaping from immune system. Besides, branch of cell fate 2 was dominated by metastatic EpiCs (Fig. 4A). Genes of cells in fate 2 enriched in biological process of cellular component organization or biogenesis (Fig. 4A, B Cluster 1). Correct and efficient assembly, arrangement and disassembly of cellular components is crucial for the cells to maintain normal physiological state. Cells in fate 2 might promote metastasis by interacting with surrounding mesenchymal cells to regulate biochemical and mechanical properties of the extracellular matrix. For genes differentially expressed between primary and metastasis, 620 genes were downregulated and 483 genes were upregulated along pseudotime trajectory (Fig. S1A). We found 4 of the top 30 markers of EC5 upregulated at the late stage

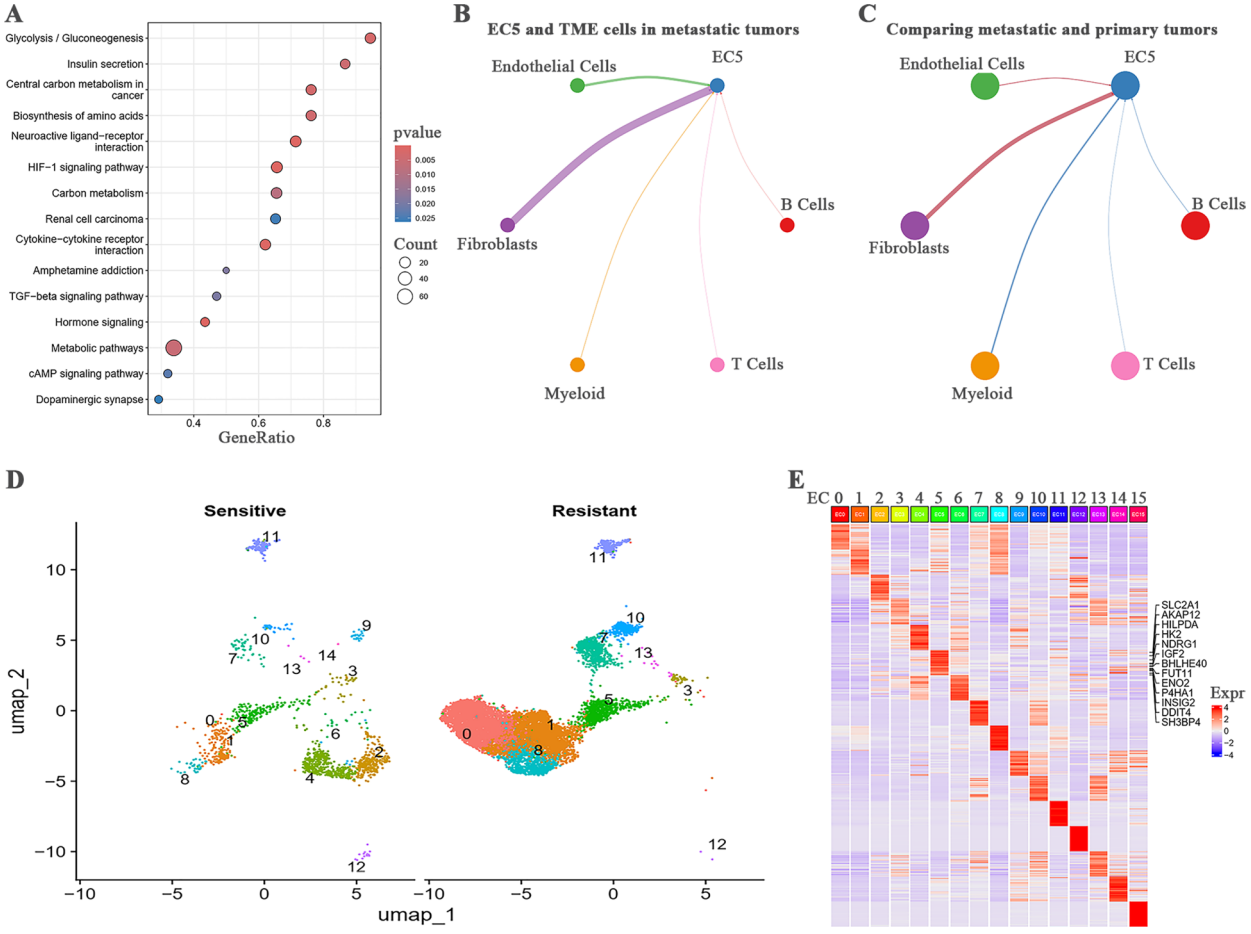

Fig. 3 EC5 communicated with mesenchymal cells and could escape immune response. **A**. KEGG pathways of subcluster EC5 determined by GSEA, including ligand/cytokine-receptor interaction related pathways, and TGF-β signaling pathway. **B**. Cell interaction strength (represented by line thickness) was high between subcluster EC5 and mesenchymal cells but low between EC5 and immune cells in metastatic tumors. Colors of lines were consistent with different cell types that interacted with EC5. **C**. Cell-cell communications between EC5 and mesenchymal cells increased (red lines) in metastasis compared with primary groups while that between EC5 and immune cells decreased (blue lines). The line thickness represented the interaction strength. **D**. Increase of EC5 in chemo-resistant samples compared with chemo-sensitive samples. **E**. Heatmap showing the expression profiles of top 30 markers of each epithelial subclusters. 13 hub genes negatively associated with prognosis in EC5 were annotated

of progression toward metastasis, including AKAP12, FUT11, NDUFA4L2, STC1.

Taking intersection among genes that were hub genes of EC5, negatively correlated with OS time, and upregulated at the late stage of pseudotime trajectory progressing toward metastasis, 2 genes were identified, including FUT11 and AKAP12 (Fig. 4C). The A-kinase anchor protein AKAP12 had been reported as a poor prognostic marker for OC. FUT11 was a fucosyltransferase less known in OC. As EC5 was found to enrich in ligand/cytokine-receptor interaction related pathways, carbohydrate metabolism pathways and some signaling pathways, we focused on the hub gene FUT11, which might modulate the activity of cytokine receptors.

We firstly confirmed the expression of FUT11 in OC. FUT11 was significantly upregulated in ovarian tumors in TCGA and GTEx cohort (Fig. 4D). Next, we validated that OC cell lines HEY and SK-OV-3 both exhibited a significantly higher FUT11 expression level (3.12±0.34 and 40.63±10.94) than normal ovarian cell line OSE (1.00±0.03) by qPCR ($p < 0.05$, Fig. 4E). We also observed a trend of upregulation of FUT11 with ages, consistent with increased risk of OC (Fig. S1B). Taken together, FUT11 was overexpressed in OC.

Then, we analyzed the impact of FUT11 on the survival of OC. A significant correlation was observed between the elevated expression of FUT11 and poor OS time in OC patients (HR=1.483 [1.123–1.959.123.959], p=0.005, Fig. 4F). This result indicated that OC patients with low FUT11 expression lived longer than those with high FUT11 expression. This was quite different from FUT8, which had a similar glycoprotein fucosyltransferase activity profile but showed a positive correlation with OS time (HR=0.676 [0.507–0.901.507.901], p=0.007, Fig. S1C). Therefore, FUT11 was a prognostic risk factor for OC patients.

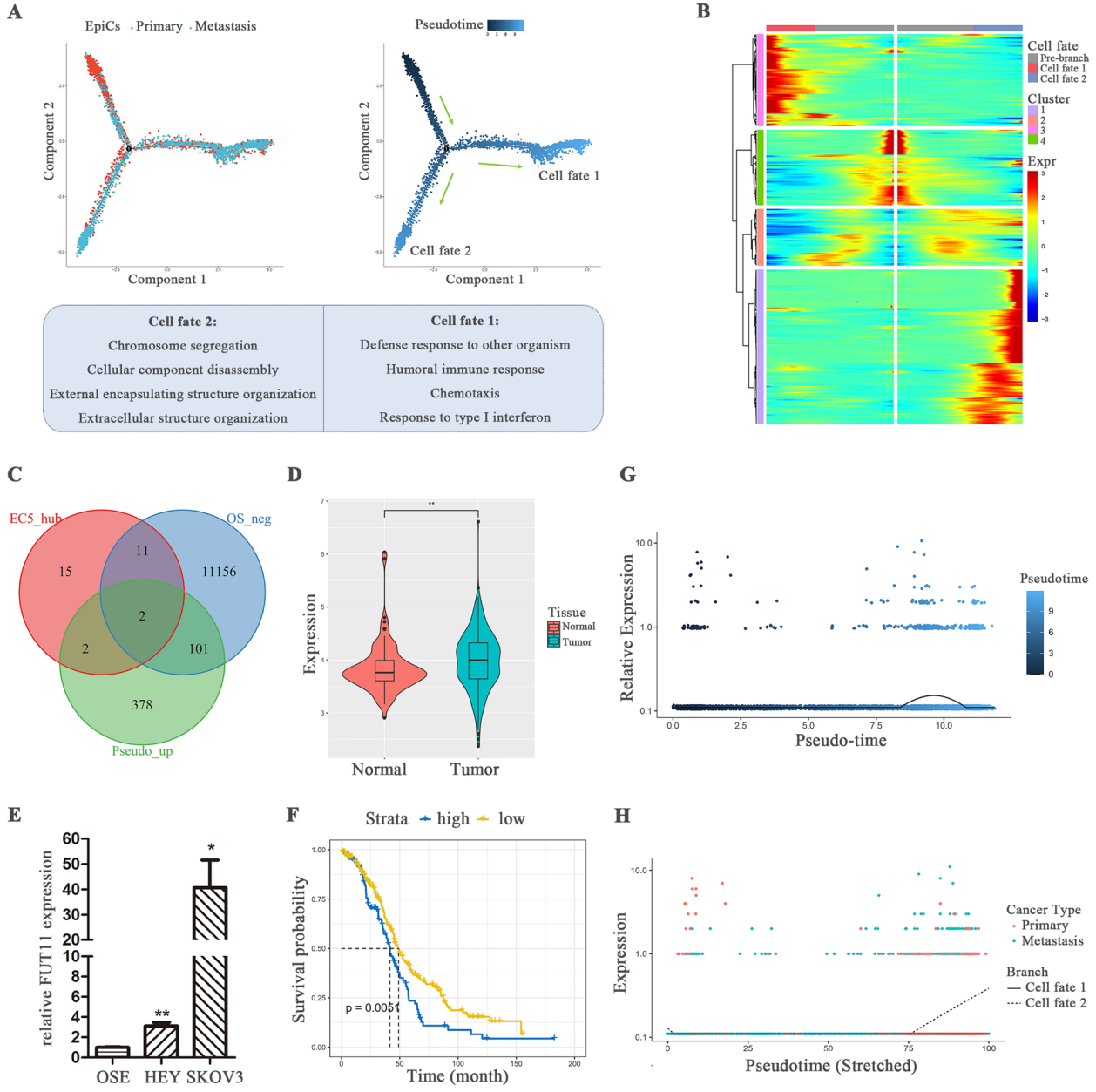

Fig. 4 FUT11 was a prognostic biomarker elevated during OC progression. **A**. Pseudotime trajectory of EpiCs inferred by Monocle2. Primary EpiCs were red-colored while metastatic EpiCs were blue-colored. Go terms related to the two potential fates were shown at the bottom. **B**. Heatmap of the dynamic changes in gene expression along the pseudotime trajectory. Gene expression varied from red (high) to blue (low). **C**. FUT11 was identified from intersection among hub genes of EC5 (EC5_hub), markers negatively correlated with OS time (OS_neg) and genes upregulated along pseudotime trajectory representing progression toward metastasis (Pseudo_up). **D**. FUT11 was upregulated in OC compared with normal ovarian samples in TCGA and GTEx cohort. Statistics was performed using Wilcoxon rank-sum test. Asterisk (**) indicates $p < 0.01$. **E**. FUT11 showed higher mRNA expression in HEY and SK-OV-3 OC cell lines compared with normal ovarian cell line OSE. **F**. Kaplan-Meier analysis of patients from TCGA cohort showed that FUT11 was negatively associated with OS time. **G**. FUT11 upregulated at late stage of tumor progression along pseudotime trajectory. **H**. FUT11 expression changed along branches in pseudotime trajectory, transiting from primary state to a metastatic state (cell fate 2)

Moreover, along the pseudotime trajectory, FUT11 was upregulated at the late stage of tumor progression (Fig. 4G). FUT11 was inferred as relevant for transition from primary state to a metastatic state that was related with cellular component organization or biogenesis (Cell fate 2), indicating that FUT11 affected tumor metastasis through interactions with mesenchymal cells (Fig. 4H).

FUT11 regulated invasion and migration in OC cells

To evaluate the role of FUT11 in tumor cell migration and invasion in vitro, we carried out siRNA experiments

in HEY and SK-OV-3. To select the most effective siRNA to downregulate FUT11 in OC, 3 siRNAs and scramble siRNA were delivered into two OC cells separately. Treatment with three FUT11 siRNAs caused 61%, 44%, and 85% significant reduction of FUT11 expression in SK-OV-3, respectively ($p < 0.05$, Fig. 5A, left). Meanwhile, administration of three FUT11 siRNAs also caused 41%, 39%, 88% reduction of FUT11 expression in HEY, respectively, although the reduction was significant only for siRNA-1 and siRNA-3 treated groups (Fig. 5A, right). Together, FUT11 siRNA-3 was used for the ongoing experiments. Downregulation of FUT11 protein expression with siRNA treatment was further confirmed by western-blot (Figs. 5B and S1D).

To evaluate the effect of FUT11 knockdown on cancer progression in SK-OV-3 and HEY cells, we conducted invasion and migration assays. The matrigel invasion assays revealed remarkable decrease in cell invasion upon FUT11 knockdown in SK-OV-3 and HEY ($p < 0.01$, Fig. 5C). FUT11 siRNA treatment also significantly impaired the migration ability of SK-OV-3 and HEY, compared with control siRNA-treated groups ($p < 0.01$, Fig. 5D). Taken together, these results showed that the expression of FUT11 was positively correlated with migration and invasion characteristics of OC.

FUT11 communicated with TME cells through TGF-β signaling pathway

We tried to elucidate the mechanisms how FUT11 regulated OC development. As FUT11 was one of the biomarkers of subcluster EC5, a similar phenomenon was observed that FUT11+ EpiCs had high interaction strength with mesenchymal cells, and this interaction increased in metastatic tissues (Fig. 6A, B). This indicated

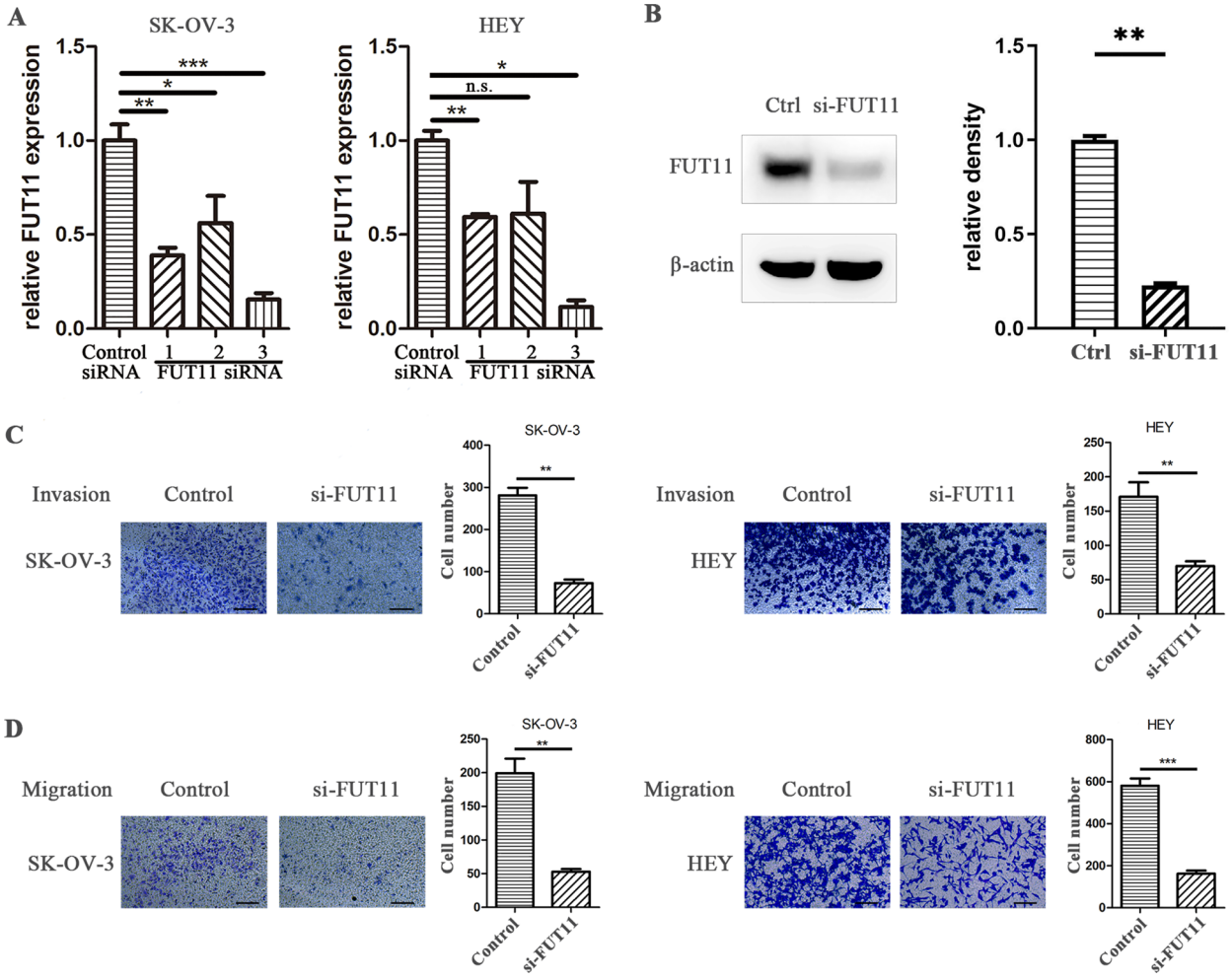

Fig. 5 Function of FUT11 in progression of OC. **A**. Effect of siRNA-mediated downregulation of FUT11 mRNA expression in SK-OV-3 and HEY cell lines. **B**. Western-blot showed that FUT11 downregulated in si-FUT11 groups compared with control (Ctrl) groups. 20 μg protein was loaded, with β-actin as loading control. **C-D**. Representative images and number of invaded (**C**) and migrated (**D**) cells in si-FUT11 and control groups. Scale bar=200 μm. Data was analyzed by Student's t test and expressed as mean ± standard deviation of three replicates. Asterisk (*) indicates $p < 0.05$ compared with control groups, while (**) indicates $p < 0.01$, (***) indicates $p < 0.001$, "n.s." indicates $p > 0.05$

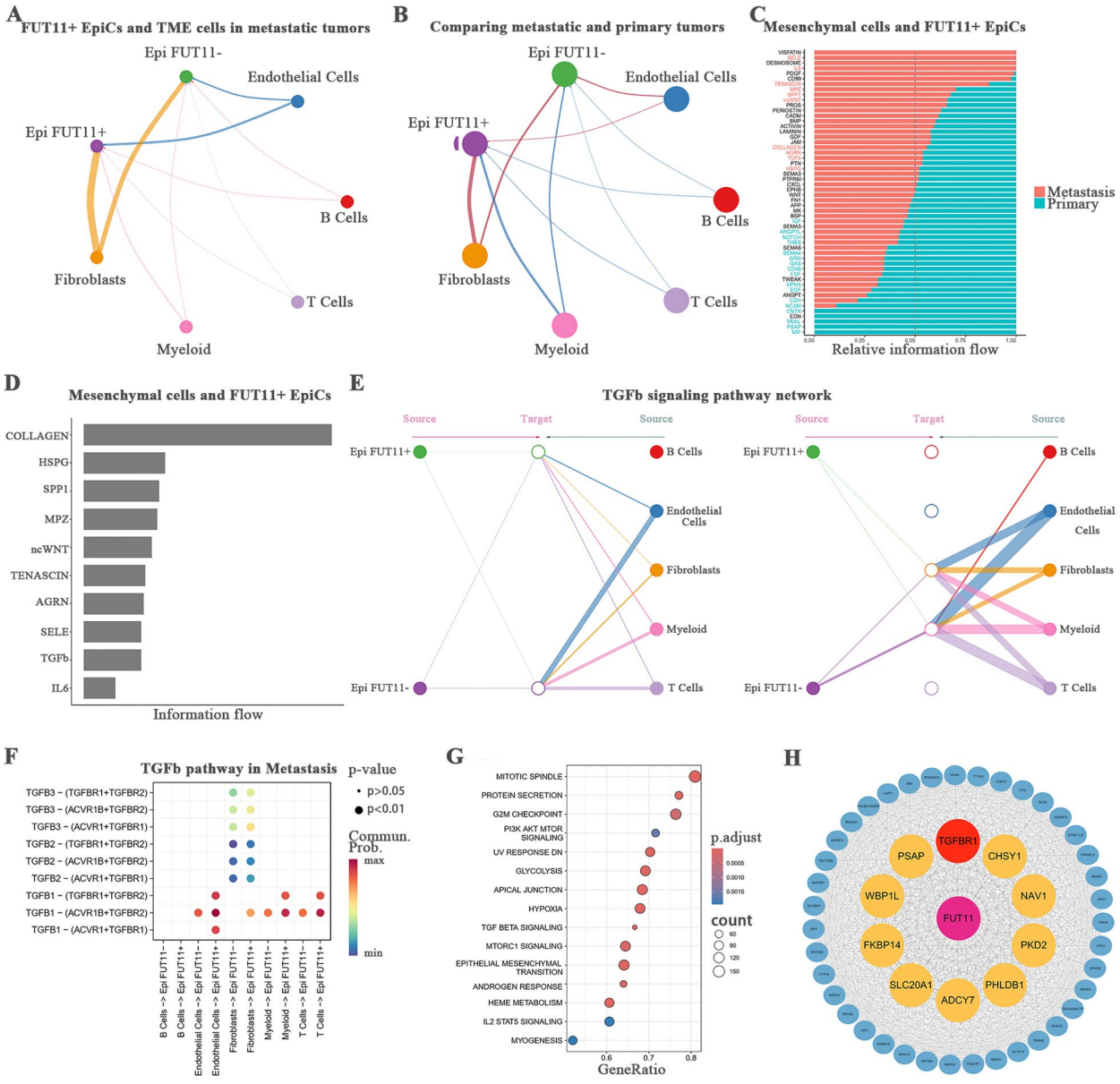

Fig. 6 FUT11 communicated with TME cells through TGF-β signaling pathway. **A**. FUT11+ EpiCs had high cell interaction strength with mesenchymal cells but low interaction strength with immune cells. **B**. Changes of cell-cell communications between FUT11+ EpiCs and mesenchymal cells increased (red lines) in metastasis compared with primary samples. **C**. Information flow of signaling pathways from mesenchymal cells to FUT11+ EpiCs in metastasis compared with primary tissues. TGF-β pathway was among the significant enriched pathways in metastasis (red annotations). **D**. Information flow of signaling pathways from mesenchymal cells to FUT11+ EpiCs in metastasis. **E**. Hierarchy plot demonstrating higher TGF-β signaling in FUT11+ EpiCs communicated with mesenchymal cells than that in FUT11- EpiCs. **F**. Bubble plots showing the ligands and receptors of TGF-β pathway. **G**. TGF-β pathway was among the top 15 pathways of FUT11 correlated genes determined by GSEA. **H**. PPI network within the genes correlated with FUT11 (purple-colored). Nodes on the inner circle indicated the top 10 hub genes (TGFBR1 was red-colored). The outer circle in blue represented other proteins

that FUT11+ EpiCs could escape immune surveillance and might promote metastasis through cellular communication with mesenchymal cells.

For communications between FUT11+ EpiCs and mesenchymal cells, high-ranking pathways that enriched in metastatic tissues included the secreted signaling interaction pathways (SPP1, ncWNT, TGF-β and IL6), the ECM-receptor interaction pathways (COLLAGEN, HSPG, TENASCIN and AGRN) as well as the cell-cell contact interaction pathways (MPZ and SELE) (Fig. 6C, D). Most of these pathways were also enriched in communications between FUT11- EpiCs and mesenchymal cells in metastatic samples by pathway enrichment analysis, except for the TGF-β pathways (Fig. S2A, S2B). Stronger TGF-β signals were observed in FUT11+ EpiCs communicated with mesenchymal cells (especially endothelial cells) than

that in FUT11- EpiCs (Fig. 6E). Therefore, we focused on mechanisms of FUT11 in regulating TGF-β pathway.

For receptor-ligand interaction analysis of the TGF-β pathway in metastasis, the ACVR1 and TGF-β receptor 1 (TGFBR1) receptors were specially expressed on FUT11+ EpiCs and bound with the TGFB1 ligands expressed by endothelial cells (Fig. 6F). Besides, when communicated with fibroblasts, the expression of ACVR1 and TGFBR1 receptors were higher in FUT11+ EpiCs than that in FUT11- EpiCs (Fig. 6F).

We also evaluated FUT11 correlated genes in OC in TCGA database. TGF-β signaling pathway were discovered among the top 15 pathways by pathway enrichment analysis (Fig. 6G). Genes with Spearman correlation coefficient $\geq$ 0.4 were predicted and the top 600 genes were selected. We surveyed the PPI network among the proteins correlated with FUT11 using the Cytoscape and identified TGFBR1 as one of the top 10 main hubs (Fig. 6H). Therefore, FUT11 regulated TGF-β pathway through TGF-β receptors.

Taken together, FUT11 regulated the progression of OC through the TGF-β signaling pathway. The TGF-β receptors played important roles in mediating intercellular interactions between EpiCs and TME cells.

Validation of FUT11 in regulating the TGF-β signaling pathway

We next confirmed the effects of FUT11 in regulating the TGF-β signaling pathway. TGFBR1 was a main hub gene that correlated with FUT11 and was important for transducing signals upon TGF-β stimulation. FUT11 displayed a positive correlation with TGFBR1, while FUT8 displayed very weak correlation with TGFBR1 (Fig. 7A, S2C). Lack of FUT11 downregulated the TGFBR1 expression in OV cells (Fig. 7B). Besides, FUT11 is positively associated with TGFBRAP1, which could stabilize TGFBR1 by inhibiting its binding with Smurf1/2 to prevent proteasomal degradation (Figure S2D). These results indicated that FUT11 regulated TGFBR1 expression.

As TGFBR1 transduced the signaling by p-SMAD3, we tested whether FUT11 facilitated SMAD3 phosphorylation and nuclear translocation upon TGFB1 treatment. We observed that p-SMAD3 distributed both in cytoplasm and nucleus in control OV cells, and was more dispersed in cytoplasm when FUT11 was knocked down (Fig. 7C, row 1–2). Upon TGFB1 treatment, p-SMAD3 accumulated in the nucleus, but FUT11 knockdown attenuated its nucleus expression (Fig. 7C, row 3–4). As a result, the expression of genes downstream of SMAD3,

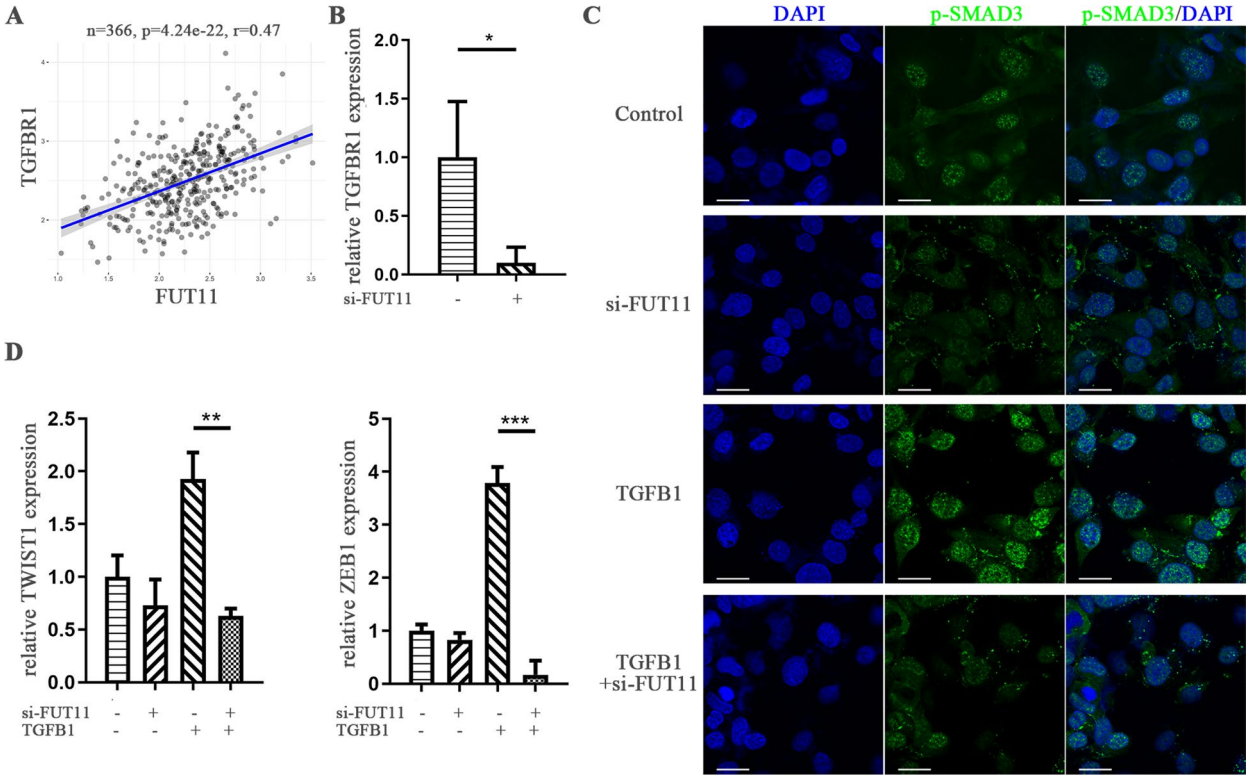

Fig. 7 Validation of FUT11 in regulating TGF-β signaling pathway. **A**. Scatter plot displayed a positive correlation between FUT11 and TGFBR1. **B**. mRNA expression of TGFBR1 downregulated in si-FUT11 groups compared with control groups. **C**. Nucleus translocation of p-SMAD3 upon TGFB1 treatment was impaired when lack of FUT11. Scale bar=30 μm. **D**. Upon TGFB1 treatment, mRNA expression of TWIST and ZEB1 downregulated in si-FUT11 groups compared with control group. Asterisk (*) indicates $p < 0.05$, Asterisk (**) indicates $p < 0.01$, while (***) indicates $p < 0.001$

such as TWIST and ZEB1 [35, 36], was also influenced by FUT11 expression (Fig. 7D).

Application of FUT11 in chemo-resistance prediction and drug discovery

As a hub gene of chemo-resistant EC5, FUT11 might be useful for drug response prediction. We used CTRP2, GDSC1 and GDSC2 datasets to analyze drug resistance due to high FUT11 expression. FUT11 expression level was significantly correlated with drug sensitivity of conventional drugs such as gemcitabine, docetaxel, carboplatin and cisplatin (Fig. 8A). Patients in FUT11-high groups in TCGA had higher IC50 and were more resistant to these drugs than FUT11-low groups (Fig. 8B). This was consistent with the upregulation of FUT11 in chemo-resistant samples compared with chemo-sensitive samples in single-cell studies (Fig. 8C). FUT11 communicated with mesenchymal cells through pathways such as TGF-β and ncWNT. In the drug discovery process, LY-2157299, a TGFBR1 kinase inhibitor that could downregulate p-SMAD2 and p-SMAD3, was identified to be more effective in the FUT11-high group (Fig. 8D). We also identified AZ6102_2109 inhibiting WNT signaling as a potential drug (Fig. 8E).

Taken together, FUT11 regulated tumor progression and drug resistance through the TGF-β/TGFBR1/SMAD3 pathway, providing novel diagnostic biomarkers and therapeutic targets for precision medicine of OC (Fig. 8F).

Discussion

Interpatient and intratumour heterogeneity of OC is caused by different origins and complex biological factors and is crucial for comprehending tumor progression and drug resistance [37, 38]. The scRNA-seq revolutionized understanding of genetic information at the cellular level across various tissues and diseases, and deciphered intercellular heterogeneity within samples [39]. Researchers had utilized scRNA-seq to characterize protein-coding and non-coding gene expression heterogeneity in immortalized, non-transformed and transformed lung epithelial cell lines [40]. Microenvironment patterns were analyzed by scRNA-seq to reflect histological grade of lung adenocarcinoma [41]. The scRNA-seq also revealed a prevalent and complex lncRNA-mediated clear cell renal cell carcinoma metastasis [42]. In order to improve the treatment effect of OC, it is an urgent need to clarify the relevant mechanisms and find effective diagnostic markers and therapeutic targets.

In this study, we explored the heterogeneity of OC samples and found diverse subclusters within EpiCs. We identified subcluster EC5 enriched in metastatic and chemo-resistant tumors and significantly associated with worse prognosis. Genes of EC5 mainly enriched in pathways such as carbohydrate metabolism pathways, ligand/cytokine-receptor interaction related pathways, and TGF-β pathways, which could fuel the bioenergetic and biosynthetic needs of tumors and encouraged metastasis and immune evasion [43, 44]. Similar as EC5, FUT11+ EpiCs had stronger interactions with mesenchymal cells than immune cells, and these interactions upregulated in metastasis. The secreted signaling interaction pathways, such as SPP1, ncWNT, TGF-β and IL6, also contributed significantly to the communications in metastasis than primary tumors. FUT11 was overexpressed in chemo-resistant cells and predictive of resistance to conventional OC drugs. These suggested that FUT11+ EpiCs interacted with mesenchymal cells and played important roles in tumor metastasis and chemo-resistance.

Besides, old age was one of the major risk factors for ovarian cancer. Old women were more likely than young women to be diagnosed with OC. We separated samples into two groups with age older or younger than 55, and observed that FUT11 was upregulated with ages. TGF-β was secreted to induce and maintain senescent phenotype and age-related pathological conditions [45]. Age-related upregulation of FUT11 assisted TGF-β to create a permissive environment for oncogenesis and affect therapeutic efficacy.

Next, diverse FUTs were involved in different kinds of tumor to affect the expression, activation and degradation of proteins, providing novel biomarkers and targets for therapeutic intervention. FUT11 was an α–1,3-FUT that might modulate the activity of cytokine receptors and lead to aberrations associated with cancer [46]. Until now, although FUT11 had been reported as a hub gene in some types of cancer [14, 16–18], functions of FUT11 in OC were less known. On the one hand, while other classical α–1,3/4-FUTs were implicated in terminal fucosylation, FUT11 had glycoprotein fucosyltransferase activity profiles similar to that of FUT8, which was usually thought as the only FUT that catalyzed core fucosylation [10, 47, 48]. FUT8 was needed for regulation of the TGF-β signaling pathway [13, 49, 50]. FUT11 might also regulate OC progression through regulating TGF-β signaling pathway. On the other hand, FUT8 was associated with poor prognosis of non-small cell lung cancer, glioma, diffuse large B cell lymphoma and BC, but with good survival in GC [49, 51, 52]. Although FUT8 was highly expressed in malignant ovarian tumors compared to benign tumors [53], we observed a significant correlations between the elevated expression of FUT8 and improved OS time in our study. This was quite different from the negative association of FUT11 with survival in OC. Furthermore, FUT11 displayed a positive correlation with TGFBR1, while FUT8 displayed very weak correlation with TGFBR1. Taken together, FUT11 might

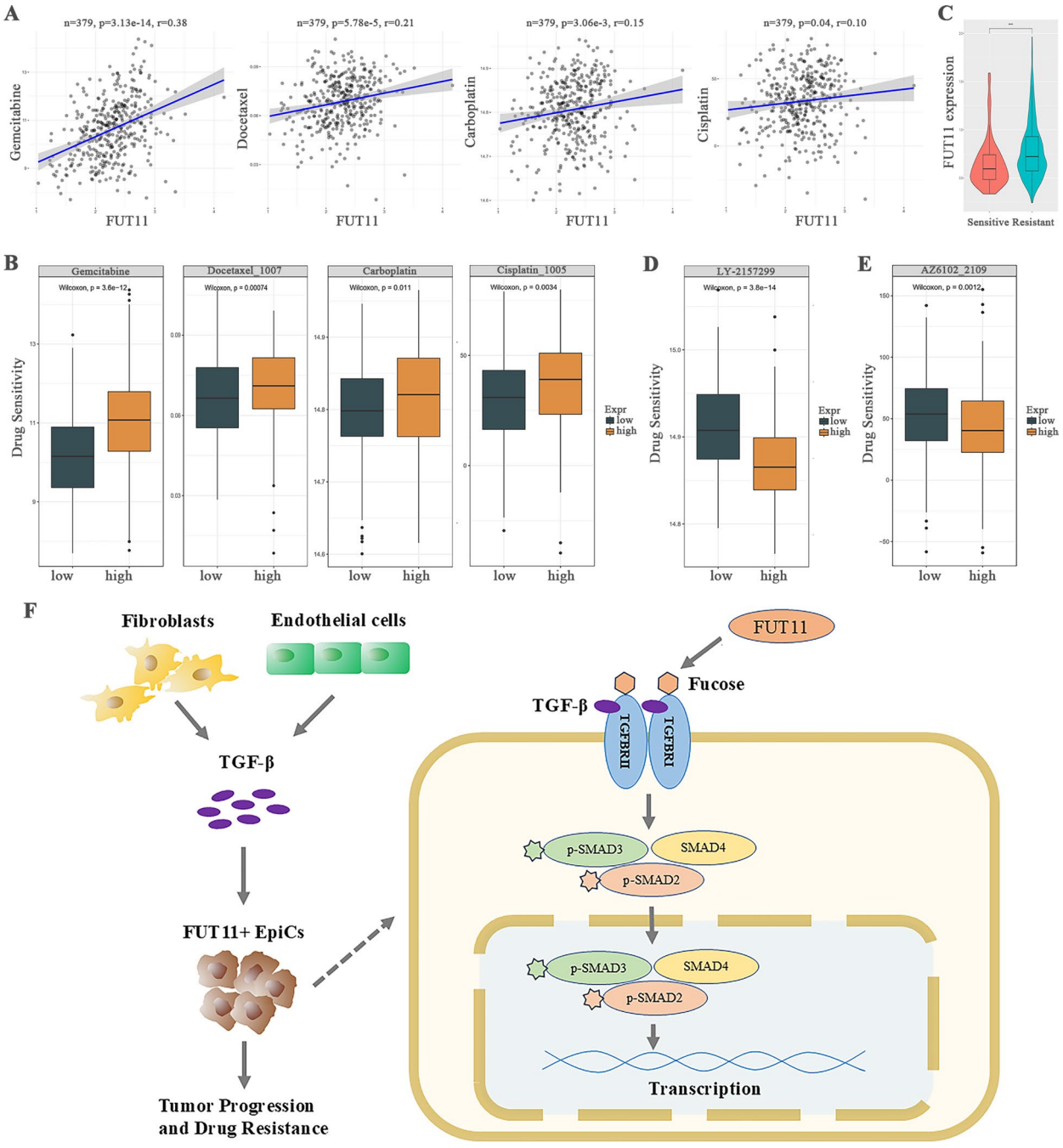

Fig. 8 Application of FUT11 in chemo-resistance prediction and drug discovery. **A**. Relationship between FUT11 expression and drug sensitivity of gemcitabine, docetaxel, carboplatin and cisplatin. **B**. Drug sensitivity showed that FUT11-high patients were more resistant to gemcitabine, docetaxel, carboplatin and cisplatin than FUT11-low groups. **C**. FUT11 was upregulated in chemo-resistant samples compared with chemo-sensitive samples in single-cell studies. Asterisk (****) indicates $p < 0.0001$. **D**. LY-2157299, a TGFBR1 kinase inhibitor downregulating p-SMAD2 and p-SMAD3, was more effective for the FUT11-high group. **E**. Potential drug targeting WNT pathway that was effective for the FUT11-high group. **F**. Proposed mechanisms and applications of FUT11 in OC diagnosis and treatment. FUT11+ EpiCs communicated with mesenchymal cells in TME through TGF-β receptors, facilitating phosphorylation and nucleus translocation of SMADs and regulation of downstream genes to promote tumor progression and drug resistance

regulate OC progression through TGF-β pathway with mechanisms not the same as FUT8.

Moreover, our study elucidated the regulatory mechanisms of FUT11 in OC progression and its potential application in chemo-resistance prediction and drug discovery. TGF-β pathway was one of the high-ranking signaling pathways that enriched in FUT11+ EpiCs communicated with mesenchymal cells. Upon TGF-β treatment, SMAD3 was phosphorylated at its extreme C terminus by TGFBR1, enabling its interaction with

SMAD4 and subsequent nuclear translocation of the complex [54, 55]. Core fucosylation was important for function of TGF-β receptors [56]. In our study, FUT11 displayed a positive correlation with TGFBR1 expression. We also observed that FUT11 regulated TGFBRAP1, which could stabilize TGFBR1 to prevent proteasomal degradation. We hypothesized that FUT11 might play a role in activation and degradation of TGF-β receptors. Besides, our study identified FUT11 as a predicator for resistance to conventional drugs and offered potential therapeutic targets in TGF-β pathway for precision medicine. Other pivotal regulators in tumor progression for therapeutic applications still remained to be unraveled. Furthermore, although we focused on the TGF-β signaling pathway in this study, other signaling pathways enriched in FUT11+ EpiCs, such as WNT pathway, were also of important research value and might provide more effective drugs.

In conclusion, this study characterized the heterogeneous TME of OC and identified a metastatic and chemo-resistant subcluster EC5. FUT11 was a hub gene of EC5 and promoted progression of OC through regulation of TGF-β receptors, facilitating phosphorylation and nucleus translocation of SMAD3 to regulate downstream genes. Our researches provided candidate diagnostic marker and effective therapeutic target for OC and extended understanding of tumor progression.

Abbreviations

OC	Ovarian cancer
scRNA-seq	Single-cell RNA sequencing
FUT11	Fucosyltransferase 11
CNV	Copy-number variations
PPI	Protein–protein interaction
FUT11+	FUT11 positive
TGF-β	Transforming growth factor-β
TME	Tumor microenvironment
EpiCs	Epithelial cells
BC	Breast cancer
GC	Gastric cancer
GEO	Gene expression omnibus
GTEx	Genotype-tissue expression
TCGA	The cancer genome atlas
GSVA	Gene set variation analysis
OS	Overall survival
KEGG	Kyoto encyclopedia of genes and genomes
GSEA	Gene set enrichment analysis
GO	Gene ontology
qPCR	Quantitative real-time PCR
TGFB1	TGF-β 1
TBST	TBS and 0.1% tween-20
IF	Immunofluorescence
SMAD3	SMAD family member 3
UMAP	Uniform manifold approximation and projection
TGFBR1	TGF-β receptor 1

Supplementary Information

The online version contains supplementary material available at https://doi.org/10.1186/s12935-026-04299-y.

Supplementary file 1.

Acknowledgements

We sincerely thank all participants from the Beijing Obstetrics and Gynecology Hospital, Capital Medical University, Beijing Maternal and Child Health Care Hospital, PR China.

Author contributions

Q. C.: conception and design of the study, acquisition and interpretation of data, drafted the work. WT. Y., M. J.: supervised the study. ZB. L., JP. W., Y. T.: acquisition of data. All authors reviewed the final manuscript.

Funding

This research was supported by the Capital's Funds for Health Improvement and Research (No. 2022-2-2116), the Beijing Obstetrics and Gynecology Hospital, Capital Medical University (No. FCYYJC202202).

Data availability

The datasets presented in this study are openly available in the GEO database (https://www.ncbi.nlm.nih.gov/geo) under accession number GSE130000, GSE201047 and GSE158937, and the BioStudies database (http://www.ebi.ac.uk/biostudies) under accession number E-MTAB-8107. Other data generated or analyzed in this study are available from the corresponding author on reasonable request.

Declarations

Ethics approval and consent to participate

The study was conducted in accordance with the guidelines outlined in the Declaration of Helsinki, which provides ethical principles for medical research involving human subjects. The study was approved by the Ethics Committee of the Beijing Obstetrics and Gynecology Hospital, Capital Medical University.

Consent for publication

Not applicable.

Competing interests

The authors declare no competing interests.

Received: 13 November 2025 / Accepted: 3 April 2026
Published online: 15 April 2026

References

1. Gjorgoska M, Rizner TL. From fallopian tube epithelium to high-grade serous ovarian cancer: a single-cell resolution review of sex steroid hormone signaling. Prog Lipid Res. 2024;96:101302. https://doi.org/10.1016/j.plipres.2024.101302.
2. Kumar S, Raina M, Tankay K, Ingle GM. Patient-derived organoids in ovarian cancer: current research and its clinical relevance. Biochem Pharmacol. 2023;213:115589. https://doi.org/10.1016/j.bcp.2023.115589.
3. Lin Q, Li J, Abudousalamu Z, Sun Y, Xue M, Yao L, et al. Advancing ovarian cancer therapeutics: the role of targeted drug delivery systems. Int J Nanomedicine. 2024;19:9351–70. https://doi.org/10.2147/IJN.S478313.
4. Mauro LJ, Spartz A, Austin JR, Lange CA. Re-evaluating the role of progesterone in ovarian cancer: is progesterone always protective? Endocr Rev. 2023;44(6):1029–46. https://doi.org/10.1210/endrev/bnad018.
5. Chai C, Liang L, Mikkelsen NS, Wang W, Zhao W, Sun C, et al. Single-cell transcriptome analysis of epithelial, immune, and stromal signatures and interactions in human ovarian cancer. Commun Biol. 2024;7(1):131. https://doi.org/10.1038/s42003-024-05826-1.
6. Liu K, Han H, Xiong K, Zhai S, Yang X, Yu X, et al. Single-cell landscape of intratumoral heterogeneity and tumor microenvironment remolding in pre-nodal metastases of breast cancer. J Transl Med. 2024;22(1):804. https://doi.org/10.1186/s12967-024-05625-6.
7. Shao W, Lin Z, Xiahou Z, Zhao F, Xu J, Liu X, et al. Single-cell RNA sequencing reveals that MYBL2 in malignant epithelial cells is involved in the development and progression of ovarian cancer. Front Immunol. 2024;15:1438198. https://doi.org/10.3389/fimmu.2024.1438198.
8. Dong M, Lu L, Xu H, Ruan Z. DC-derived CXCL10 promotes CTL activation to suppress ovarian cancer. Transl Res. 2024;272:126–39. https://doi.org/10.1016/j.trsl.2024.05.013.

9. Xu J, Lu W, Wei X, Zhang B, Yang H, Tu M, et al. Single-cell transcriptomics reveals the aggressive landscape of high-grade serous carcinoma and therapeutic targets in tumor microenvironment. Cancer Lett. 2024;593:216928. https://doi.org/10.1016/j.canlet.2024.216928.
10. Mollicone R, Moore SE, Bovin N, Garcia-Rosasco M, Candelier JJ, Martinez-Duncker I, et al. Activity, splice variants, conserved peptide motifs, and phylogeny of two new alpha1,3-fucosyltransferase families (FUT10 and FUT11). J Biol Chem. 2009;284(7):4723–38. https://doi.org/10.1074/jbc.M809312200.
11. Li Z, Zhang N, Dong Z, Wang X, Zhou J, Gao J, et al. Integrating transcriptomics, glycomics and glycoproteomics to characterize hepatitis B virus-associated hepatocellular carcinoma. Cell Commun Signal. 2024;22(1):200. https://doi.org/10.1186/s12964-024-01569-y.
12. Liu Q, Adhikari E, Lester DK, Fang B, Johnson JO, Tian Y, et al. Androgen drives melanoma invasiveness and metastatic spread by inducing tumorigenic fucosylation. Nat Commun. 2024;15(1):1148. https://doi.org/10.1038/s41467-024-45324-w.
13. Tu CF, Wu MY, Lin YC, Kannagi R, Yang RB. FUT8 promotes breast cancer cell invasiveness by remodeling TGF-β receptor core fucosylation. Breast Cancer Res. 2017;19(1):111. https://doi.org/10.1186/s13058-017-0904-8.
14. Wang P, Liu X, Yu J, Meng Z, Lv Z, Shang C, et al. Fucosyltransferases Regulated by Fusobacterium Nucleatum and Act as Novel Biomarkers in Colon Adenocarcinoma. J Inflamm Res. 2023;16:747–68. https://doi.org/10.2147/JIR.S396484.
15. Zhu Y, Zhao Y, Cao Z, Chen Z, Pan W. Identification of three immune subtypes characterized by distinct tumor immune microenvironment and therapeutic response in stomach adenocarcinoma. Gene. 2022;818:146177. https://doi.org/10.1016/j.gene.2021.146177.
16. Carrascal MA, Silva M, Ramalho JS, Pen C, Martins M, Pascoal C, et al. Inhibition of fucosylation in human invasive ductal carcinoma reduces E-selectin ligand expression, cell proliferation, and ERK1/2 and p38 MAPK activation. Mol Oncol. 2018;12(5):579–93. https://doi.org/10.1002/1878-0261.12163.
17. Zhang X, Wang Y. Identification of hub genes and key pathways associated with the progression of gynecological cancer. Oncol Lett. 2019;18(6):6516–24. https://doi.org/10.3892/ol.2019.11004.
18. Cao W, Zeng Z, Pan R, Wu H, Zhang X, Chen H, et al. Hypoxia-related gene FUT11 promotes pancreatic cancer progression by maintaining the stability of PDK1. Front Oncol. 2021;11:675991. https://doi.org/10.3389/fonc.2021.675991.
19. Ruan W, Yang Y, Yu Q, Huang T, Wang Y, Hua L, et al. FUT11 is a target gene of HIF1alpha that promotes the progression of hepatocellular carcinoma. Cell Biol Int. 2021;45(11):2275–86. https://doi.org/10.1002/cbin.11675.
20. Zhang B, Chen Y, Gu X, Zheng Y, Jiang ZH. Fucosyltransferase 11 restrains ferroptosis via upregulation GPX4 expression in gastric cancer. BMC Cancer. 2025;25(1):923. https://doi.org/10.1186/s12885-025-14340-4.
21. Cao W, Zeng Z, Lan J, Yang Y, Lu M, Lei S. Knockdown of FUT11 inhibits the progression of gastric cancer via the PI3K/AKT pathway. Heliyon. 2023;9(7):e17600. https://doi.org/10.1016/j.heliyon.2023.e17600.
22. Chen Q, Gao Y, Yue W. Delineating the mechanisms of alpha 1-3 fucosyltransferase FUT11 in ovarian cancer. Ann Oncol. 2019;30(suppl_5):v10.
23. Gene expression omnibus database. https://www.ncbi.nlm.nih.gov/geo. Accessed 28 Dec 2023.
24. Barrett T, Wilhite SE, Ledoux P, Evangelista C, Kim IF, Tomashevsky M, et al. NCBI GEO: archive for functional genomics data sets–update. Nucleic Acids Res. 2013;41(Database issue):D991-5. https://doi.org/10.1093/nar/gks1193.
25. BioStudies database. http://www.ebi.ac.uk/biostudies. Accessed 6 Dec 2024.
26. Sarkans U, Gostev M, Athar A, Behrangi E, Melnichuk O, Ali A, et al. The BioStudies database-one stop shop for all data supporting a life sciences study. Nucleic Acids Res. 2018;46(D1):D1266-70. https://doi.org/10.1093/nar/gkx965.
27. Hao Y, Stuart T, Kowalski MH, Choudhary S, Hoffman P, Hartman A, et al. Dictionary learning for integrative, multimodal and scalable single-cell analysis. Nat Biotechnol. 2024;42(2):293–304. https://doi.org/10.1038/s41587-023-01767-y.
28. UCSC Xena. http://xena.ucsc.edu. Accessed 26 April 2023.
29. UniProt C. UniProt: the universal protein knowledgebase in 2023. Nucleic Acids Res. 2023;51(D1):D523-31. https://doi.org/10.1093/nar/gkac1052.
30. Xu S, Hu E, Cai Y, Xie Z, Luo X, Zhan L, et al. Using clusterProfiler to characterize multiomics data. Nat Protoc. 2024;19(11):3292–320. https://doi.org/10.1038/s41596-024-01020-z.
31. Hanzelmann S, Castelo R, Guinney J. GSVA: gene set variation analysis for microarray and RNA-seq data. BMC Bioinformatics. 2013;14:7. https://doi.org/10.1186/1471-2105-14-7.
32. Trapnell C, Cacchiarelli D, Grimsby J, Pokharel P, Li S, Morse M, et al. The dynamics and regulators of cell fate decisions are revealed by pseudotemporal ordering of single cells. Nat Biotechnol. 2014;32(4):381–6. https://doi.org/10.1038/nbt.2859.
33. Jin S, Guerrero-Juarez CF, Zhang L, Chang I, Ramos R, Kuan CH, et al. Inference and analysis of cell-cell communication using Cell Chat. Nat Commun. 2021;12(1):1088. https://doi.org/10.1038/s41467-021-21246-9.
34. Shannon P, Markiel A, Ozier O, Baliga NS, Wang JT, Ramage D, et al. Cytoscape: a software environment for integrated models of biomolecular interaction networks. Genome Res. 2003;13(11):2498–504. https://doi.org/10.1101/gr.1239303.
35. Cai W, Zhang Q. The transcription factor ZEB1 mediates the progression of epithelial ovarian cancer by promoting the transcription of CircANKRD17. J Biochem Mol Toxicol. 2022;36(8):e23086. https://doi.org/10.1002/jbt.23086.
36. Zhao B, Liu L, Mao J, Zhang Z, Wang Q, Li Q. PIM1 mediates epithelial-mesenchymal transition by targeting Smads and c-Myc in the nucleus and potentiates clear-cell renal-cell carcinoma oncogenesis. Cell Death Dis. 2018;9(3):307. https://doi.org/10.1038/s41419-018-0348-9.
37. Li S, Wang Z, Huang HD. Deciphering ovarian cancer heterogeneity through spatial transcriptomics, single-cell profiling, and copy number variations. PLoS One. 2025;20(3):e0317115. https://doi.org/10.1371/journal.pone.0317115.
38. Veneziani AC, Gonzalez-Ochoa E, Alqaisi H, Madariaga A, Bhat G, Rouzbahman M, et al. Heterogeneity and treatment landscape of ovarian carcinoma. Nat Rev Clin Oncol. 2023;20(12):820–42. https://doi.org/10.1038/s41571-023-00819-1.
39. Wu X, Yang X, Dai Y, Zhao Z, Zhu J, Guo H, et al. Single-cell sequencing to multi-omics: technologies and applications. Biomark Res. 2024;12(1):110. https://doi.org/10.1186/s40364-024-00643-4.
40. Moeng S, Chamorro-Parejo AD, Jeon MS, Cai JJ, Ramos KS. Single-cell RNA sequencing reveals extensive heterogeneity and unique gene trajectories in non-transformed and transformed human lung epithelial cells: insights into the role of LncRNAs in tumor heterogeneity. Int J Mol Sci. 2025;26(4):1690. https://doi.org/10.3390/ijms26041690.
41. Bischoff P, Trinks A, Obermayer B, Pett JP, Wiederspahn J, Uhlitz F, et al. Single-cell RNA sequencing reveals distinct tumor microenvironmental patterns in lung adenocarcinoma. Oncogene. 2021;40(50):6748–58. https://doi.org/10.1038/s41388-021-02054-3.
42. Li X, Meng X, Wei C, Zhou Y, Chen H, Huang H, et al. Dissecting LncRNA roles in renal cell carcinoma metastasis and characterizing genomic heterogeneity by single-cell RNA-seq. Mol Cancer Res. 2018;16(12):1879–88. https://doi.org/10.1158/1541-7786.MCR-17-0776.
43. Dalpati N, Rai SK, Sharma P, Sarangi PP. Integrins and integrin-driven secretory pathways as multi-dimensional regulators of tumor-associated macrophage recruitment and reprogramming in tumor microenvironment. Matrix Biol. 2025;135:55–69. https://doi.org/10.1016/j.matbio.2024.12.003.
44. Krieg S, Fernandes SI, Kolliopoulos C, Liu M, Fendt SM. Metabolic signaling in cancer metastasis. Cancer Discov. 2024;14(6):934–52. https://doi.org/10.1158/2159-8290.CD-24-0174.
45. Tominaga K, Suzuki HI. TGF-beta Signaling in Cellular Senescence and Aging-Related Pathology. Int J Mol Sci. 2019;20(20). https://doi.org/10.3390/ijms20205002.
46. Zhang X, Chen F, Petrella A, Chacon-Huete F, Covone J, Tsai TW, et al. A high-throughput glycosyltransferase inhibition assay for identifying molecules targeting fucosylation in cancer cell-surface modification. ACS Chem Biol. 2019;14(4):715–24. https://doi.org/10.1021/acschembio.8b01123.
47. Garcia-Garcia A, Serna S, Yang Z, Delso I, Taleb V, Hicks T, et al. FUT8-directed core fucosylation of N-glycans is regulated by the glycan structure and protein environment. ACS Catal. 2021;11(15):9052–65. https://doi.org/10.1021/acscatal.1c01698.
48. Tada K, Ohta M, Hidano S, Watanabe K, Hirashita T, Oshima Y, et al. Fucosyltransferase 8 plays a crucial role in the invasion and metastasis of pancreatic ductal adenocarcinoma. Surg Today. 2020. https://doi.org/10.1007/s00595-019-01953-z.
49. Bastian K, Scott E, Elliott DJ, Munkley J. FUT8 alpha-(1,6)-fucosyltransferase in cancer. Int J Mol Sci. 2021. https://doi.org/10.3390/ijms22010455.
50. Wang X, Inoue S, Gu J, Miyoshi E, Noda K, Li W, et al. Dysregulation of TGF-β1 receptor activation leads to abnormal lung development and emphysema-like phenotype in core fucose-deficient mice. Proc Natl Acad Sci U S A. 2005;102(44):15791–6. https://doi.org/10.1073/pnas.0507375102.
51. Li Z, Zhu Z, Wang P, Hou C, Ren L, Xu D, et al. Diagnostic, prognostic, and immunological roles of FUT8 in lung adenocarcinoma and lung squamous

cell carcinoma. PLoS One. 2025;20(5):e0321756. https://doi.org/10.1371/journal.pone.0321756.
52. Ma M, Han G, Wang Y, Zhao Z, Guan F, Li X. Role of FUT8 expression in clinicopathology and patient survival for various malignant tumor types: a systematic review and meta-analysis. Aging Albany NY. 2020;13(2):2212–30. https://doi.org/10.18632/aging.202239.
53. Yang Y, Wang M, Chen L, Chen X, Wang Y, Ye W. Clinicopathologic significance of FUT8, STX4, and calpain2 expression in ovarian cancer. Am J Transl Res. 2025;17(1):144–61. https://doi.org/10.62347/SQKL1957.
54. Shen X, Hu PP, Liberati NT, Datto MB, Frederick JP, Wang XF. Tgf-beta-induced phosphorylation of Smad3 regulates its interaction with coactivator p300/CREB-binding protein. Mol Biol Cell. 1998;9(12):3309–19. https://doi.org/10.1091/mbc.9.12.3309.
55. Wang N, Deng Y, Liu A, Shen N, Wang W, Du X, et al. Novel mechanism of the pericyte-myofibroblast transition in renal interstitial fibrosis: core fucosylation regulation. Sci Rep. 2017;7(1):16914. https://doi.org/10.1038/s41598-017-17193-5.
56. Zhang J, Ten Dijke P, Wuhrer M, Zhang T. Role of glycosylation in TGF-β signaling and epithelial-to-mesenchymal transition in cancer. Protein Cell. 2021;12(2):89–106. https://doi.org/10.1007/s13238-020-00741-7.

Publisher's Note